12^{th} International Conference on Fracture Mechanics of Concrete and Concrete Structures
FraMCoS-12
B.L.A. Pichler, Ch. Hellmich, P. Preinstorfer (Eds)

https://doi.org/10.21012/FC12.1161
MS09-2:2

CONSTITUTION OF AN EXTENSIVE EXPERIMENTAL DATABASE FOR THE CHALLENGE OF SPALLING MODELLING

J. MOUNIER[1,2], G. SCIUME[1,2,3] AND JC. MINDEGUIA[1,2]

[1] Univ. Bordeaux, CNRS, Bordeaux INP, I2M, UMR 5295, France

[2] Arts et Metiers Institute of Technology, CNRS, Bordeaux INP, Hesam Universite, I2M, UMR 5295, France

[3] Institut universitaire de France (IUF), France

Key words: Reference mortar, Temperature, Mechanical properties, Transport properties

Abstract. This study addresses the challenges of understanding the complex mechanisms of concrete behavior under fire, particularly damage and spalling. Using a standardized mortar, extensive thermal, mechanical, transport and microstructural characterizations were conducted to provide input data for a thermo-hygro-chemo-mechanical model. Preliminary results highlight the impact of elevated temperatures on the integrity of mortar, providing insight into the degradation mechanisms that affect its structural performance under thermal stress.

1 INTRODUCTION

Concrete structures, widely used in modern infrastructure, often face extreme conditions such as fires. Under high temperatures, concrete undergoes complex degradations, including cracking, loss of strength, and, in some cases, spalling. Spalling, characterized by the sudden ejection of concrete fragments, poses an immediate threat to structural and human safety while complicating fire management. Understanding these mechanisms remains challenging due to the numerous interdependent factors involved, such as permeability, thermal and moisture transfers, and mechanical stresses [15].

In this context, our study aims to address these challenges through a methodological approach. We have chosen to work with a reference material, a standardized ordinary cement mortar (according to EN 196-1 [2]), to ensure reproducibility across laboratories and minimize variations related to aggregate composition, reducing the Representative Elementary Volume (REV). While EN 196-1 specifies the granulometry and dosage of the silica, it does not detail its petrographic nature; in most cases, it is predominantly composed of quartz, which can be confirmed through thermogravimetric analysis (TGA).

Although mortar does not fully capture the behavior of concrete at high temperatures, particularly due to thermal mismatch effects, it provides a controlled and reproducible system to validate the theoretical framework of our model, especially concerning mass transfer properties. To complement this approach, we are also conducting parallel studies on a microconcrete.

The objective is to achieve a comprehensive experimental characterization of mortar exposed to high temperatures. This includes analyzing thermal properties, mass transports properties, mechanical properties, and microstructural evolution. These data will serve as the foundation for developing the constitutive equations of a thermo-hygro-chemo-

mechanical model capable of simulating the material's behavior under high temperatures.

This paper provides an overview of the experimental results of this study.

2 Materials

The mortar mix investigated, detailed in Table 1, was designed to ensure reproducibility, following standardized proportions: CEM II 32.5 cement, sand compliant with [2], and a water-to-cement (w/c) ratio of 0.5. The cement consists of 82% clinker with additions of limestone, slag, ashes and silica fume about 18%.

Cylindrical specimens (4×6 cm, 4.5×10 cm) and prismatic specimens (4×4×16 cm) were molded, covered with plastic sheets, and cured at ambient temperature for 24 hours. Subsequently, they were immersed in water for 28 days to ensure consistent curing. This duration is sufficient to achieve mechanical stability, as hydration reaches approximately 90% completion within the first 10 days [1]. Mechanical and transport tests were conducted following standard recommendations to guarantee reproducibility and reliability of results.

Table 1: Composition of the mortar mix.

Component	Quantity kg/m^3
CEM II 32.5 R	450
Sand (EN 196-1)	1350
Water	225
Water/Cement	0.5

3 Methods

Table 2 provides a summary of the tests scheduled for the characterization of the analyzed mortar. This paper focuses on presenting the results of selected tests, including TGA/DSC for thermal and chemical analysis, mechanical evaluations (bending and compression), and assessments of heat and mass transport properties, such as water porosity, mercury intrusion porosimetry, and thermal properties. When applicable, references to standard methods have been included [2], [5].

Properties	Test Type	Sample Type
Mechanical	Three points bending test	Prismatic
	Compression test	Cylinder
	Direct tensile strength	Dumbbell
Transport	Water porosity	Cylinder
	Mercury porosity	Fragments
	Unsteady Permeability	Cylinder
	Desorption Isotherm	Fragments
	Thermal Properties	Cylinder
	TGA / DSC	Pieces

Table 2: Tests carried out for characterization

3.1 Thermal preconditioning

A thermal pre-conditioning on mortar specimens is performed to study the effects of temperature on their properties and microstructure. The specimens are pre-conditioned at temperatures of 120°C, 300°C, 400°C, and 600°C, with a reference state defined at 80°C. These specific temperatures were selected to capture progressive microstructural changes while ensuring practical experimental intervals. Our choice of temperatures aims to balance experimental feasibility and the characterization of critical transformations. For instance, 120°C encompasses early dehydration phenomena, while 300°C and 400°C allow for the study of progressive dehydroxylation before the complete breakdown of portlandite near 475°C. Finally, 600°C includes both the portlandite transformation and the $\alpha - \beta$ quartz transition (573°C), making it a key stage in high-temperature performance assessment. During pre-conditioning, a temperature ramp of 1°C/min is applied to minimize thermal gradients between the core and the surface of the specimens. This gradual heating ensures uniform heat distribution, which is essential for accurate analysis of microstructural modifications [3]. Once the target temperature is reached, the specimens are held at these temperatures for specific durations (as shown in Table 3) to achieve thermal homogeneity.

T_{max} (° C)	120	300	400	600
t_{hold}(h)	10	8	6	4

Table 3: Maintaining time for preconditioning temperatures

Although the pre-conditioning process exposes the specimens to elevated temperatures, the actual tests are conducted at room temperature. This approach allows for the assessment of residual properties after thermal exposure. Future experiments are planned at moderately elevated temperatures to explore whether the residual properties can be used to model fire behavior. These models would incorporate the effects of temperature on physical parameters related to water.

3.1.1 TGA/ DSC

Thermogravimetric analysis (TGA) and differential scanning calorimetry (DSC) were performed using a Mettler Toledo TGA/DSC 3+. The aim was to examine changes in mass and heat flow in mortar under transient heating, highlighting decomposition phases and moisture loss. A completely dried sample was tested. Fragments of samples, prepared from prismatic mortar specimens, were heated at a rate of 20°C/min up to 950°C under a nitrogen atmosphere.

3.2 Mechanical tests

3.2.1 Three Points bending test

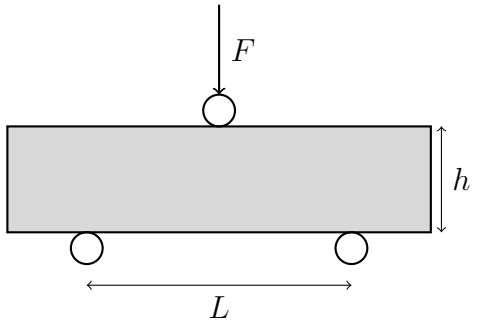

Figure 1: Schema of a three-point bending setup

The bending strength of the mortar was evaluated using a three-point bending test on prismatic specimens (160 x 40 x 40 mm), conducted according to the procedure outlined in [2]. This method was prioritized for its simplicity and reliability, with direct tensile tests planned for a later stage.

The specimens were supported on two points spaced 140 mm apart, and a vertical load was applied at the center at a displacement rate of 0.15 mm/min. The central deflection was monitored using a Linear Variable Differential Transformer (LVDT), ensuring precise measurement.

bending strength, calculated using the formula below, provides an indirect measure of the material's tensile strength:

$$R_f = \frac{3FL}{2h^3} \tag{1}$$

Here, F is the maximum load applied, L is the span length (140 mm), and h is the specimen height (40 mm). This approach allows for the characterization of tensile behavior indirectly through bending, making it a practical choice for initial evaluations.

3.2.2 Compression test

The compression test was performed on cylindrical specimens with a diameter of 45 mm and a height of 90 mm, utilizing a hydraulic press. Longitudinal deformations were recorded using three "HBM" sensors, which were affixed with elastic bands and strategically positioned at 120° increments around the specimen's mid-height. This arrangement ensured a comprehensive representation of the axial behavior. The cylindrical geometry was selected instead of the conventional 'semi-prismatic' shape advocated by standards, to allow the ongoing development of a new method for transverse strain measurement.

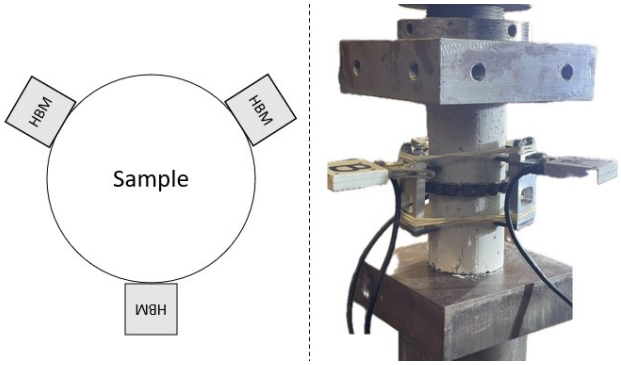

Figure 2: Compression test set up

3.3 Tests for heat and mass transport properties

The porosity of concrete can be studied using two experimental techniques [4].

3.3.1 Water porosity

This technique measures the total water-accessible porosity of the tested sample, primarily capturing capillary porosity. The water porosity of the mortar, ε_w, was determined on cylindrical specimens (40 mm diameter, 50 mm height) following AFREM recommendations [5]. The calculation is based on Equation 2:

$$\varepsilon_w = \frac{V^w}{V^{tot}} \tag{2}$$

with $V^w = \frac{m^{sat} - m^{sec}}{\rho^w}$.

ε_w is represented as a percentage based on the volumetric ratio, whereby V_w denotes the volume of water and V^{tot} signifies the total volume. Moreover, m^{sec} refers to the dry mass post-oven drying at 80°C, ρ^w indicates the density of water, and m^{sat} pertains to the mass measured in air after saturation, with surface water removed.

3.3.2 Mercury intrusion porosimetry

Mercury intrusion porosimetry (MIP) is a technique used to determine the pore size distribution, total porosity, and connectivity of porous materials. The method involves placing the sample under vacuum and progressively injecting mercury, a non-wetting liquid with a contact angle θ, into the pores. Mercury does not spontaneously enter the pores; increasing external pressure P is applied to force it in, and the cumulative mercury volume V_p (equivalent to the pore volume) is recorded at each pressure step.

The relationship between pore radius r and the applied pressure P is described by the Washburn equation:

$$r = -\frac{2\gamma \cos\theta}{P} \tag{3}$$

Here, γ is the surface tension of mercury. Assuming cylindrical pore geometry, this equation allows for the determination of the average pore radius for each pressure increment.

The global mercury (Hg porosity can also be calculated with the equation:

$$\varepsilon_{Hg} = \rho_{app} V_p \tag{4}$$

where ρ_{app} is the apparent density of the material .

3.4 Thermal properties

The experimental setup utilizes the Transient Plane Source (TPS) method, developed at Chalmers University of Technology [6]. A thin nickel spiral disk, known as the "Hot Disk," functions as both a constant-current heat source and a resistive thermometer. The disk is coated with insulating layers and placed between two test samples.

During measurement, a current pulse heats the disk, and its electrical resistance is continuously monitored and converted to temperature based on nickel's temperature-resistance relationship. Thermal conductivity is determined through inverse analysis using dedicated software.

For accurate results, the sample surfaces in contact with the disk were precision-ground to ensure flatness, minimizing air gaps. Each sample (40 mm diameter, 20 mm height) was sliced from larger cylindrical specimens (40 mm diameter, 40 mm height) and dried.

In addition to these thermal conductivity measurements, we plan to conduct Dynamic Vapor Sorption (DVS) tests and unsteady-state permeability measurements. These complementary experiments will provide further insights into the transport properties of the mortar.

4 Results and discussion

4.1 TGA/ DSC

The combined TGA/DSC analysis of the dry mortar specimen (Fig. 3) provides valuable insights into the thermal behavior of the material and its progressive degradation under increasing temperatures. The results show distinct thermal events, each corresponding to physical and chemical transformations in the mortar's microstructure.

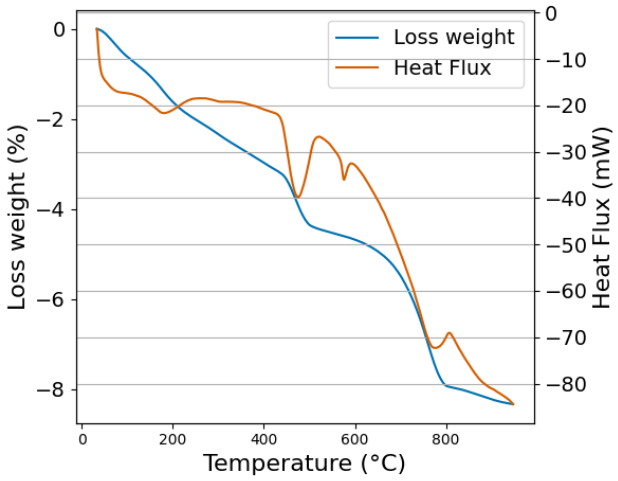

Figure 3: TGA/DSC of mortar.

The initial mass loss observed corresponds to the evaporation of free water. The specimen's behavior isolates the intrinsic thermal effects, independent of external water. This indicates the role of residual free water in early-stage thermal exposure, even in supposedly dry conditions.

At approximately 200°C, the DSC curve identifies the dehydration of hydrated calcium monocarboaluminate [7]. This reaction, while less significant in terms of mass loss, marks the onset of structural transformations that can weaken the cohesion of the matrix.

The most prominent feature in the DSC curve is the sharp endothermic peak around 475°C, corresponding to the dehydroxylation of portlandite (CH) [8]. This phase change is critical, as it directly affects the structural integrity of the mortar. The accompanying mass loss in the TGA curve underscores the significant reduction in chemically bound water at this stage.

Another distinct endothermic peak at approximately 573°C indicates the $\alpha - \beta$ quartz phase transition within the sand component [9]. Although this transformation does not contribute directly to mass loss, it reflects changes in the mechanical properties of the material due to the thermal expansion and reorganization of silica-based components.

The final major event, occurring around 770°C, is the decarbonation of calcium carbonate. This reaction represents a stage in the material's thermal degradation, as it contributes to a substantial mass loss in the TGA curve and signals the breakdown of the mortar's core structural components. By this point, the C-S-H gel and most hydration products have decomposed, leaving a weakened and porous structure with diminished mechanical stability.

4.2 Mechanical tests

4.2.1 Bending test

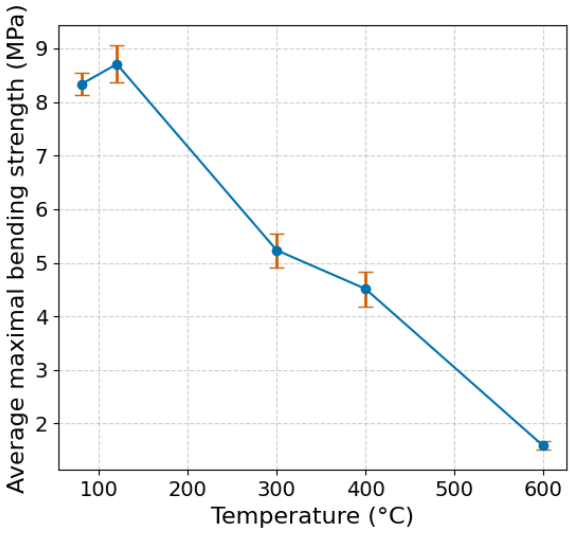

Figure 4: Evolution of bending strength by temperature

By employing the bending strength formula 1 on the experimental data, the maximum stress at various temperatures was determined. This formula presupposes a linear elastic behavior of the material under bending, which renders it a

widely accepted method for evaluating the tensile capacity of materials such as mortar and concrete. Bending strength, as derived, represents the material's capability to withstand bending-induced tensile stresses, serving as an indirect measure of its tensile strength. The average maximum stress and its standard deviation were computed for each temperature, and the results are depicted in Figure 4, demonstrating the trend of bending strength with increasing temperature.

The data reveal a reduction in bending strength as temperature rises. Notably, specimens tested immediately after thermal exposure at 600°C and cooling exhibited considerably lower strength compared to 80°C. This decline is likely tied to the loss of bending capacity resulting from thermal-induced microstructural damage (coupled effect of dehydration of cement paste and differential thermal expansion between paste and sand grains).

These findings align with the TGA-DSC results (Figure 3), which reveal the decomposition of hydration phases such as portlandite and C-S-H gel at elevated temperatures. The thermal degradation of these phases contributes to the loss of structural integrity, reducing the material's ability to withstand tensile stresses during bending.

Compared to concrete, mortar exhibits a more pronounced reduction in mechanical strength at high temperatures. This difference can be attributed to the absence of coarse aggregates, which, in concrete, act as a rigid skeleton that helps maintain structural integrity. In contrast, mortar, composed solely of cement paste and sand, is more susceptible to dehydration effects and the thermal mismatch between paste and sand grains. This mismatch generates additional internal stresses, accelerating damage and leading to a greater loss of mechanical properties. Furthermore, the higher proportion of cementitious phases in mortar amplifies the effects of phase decomposition (portlandite, C-S-H), directly impacting its compressive strength and modulus of elasticity.

4.2.2 Compression test

Figure 5 shows the average maximal compressive strength as a function of temperature. Like bending strength, compressive strength initially increases up to 120°C due, probably, to pore water loss and improved microstructure densification, before rapidly declining beyond 300°C. At 600°C, the strength falls below 10 MPa, indicating severe structural degradation.

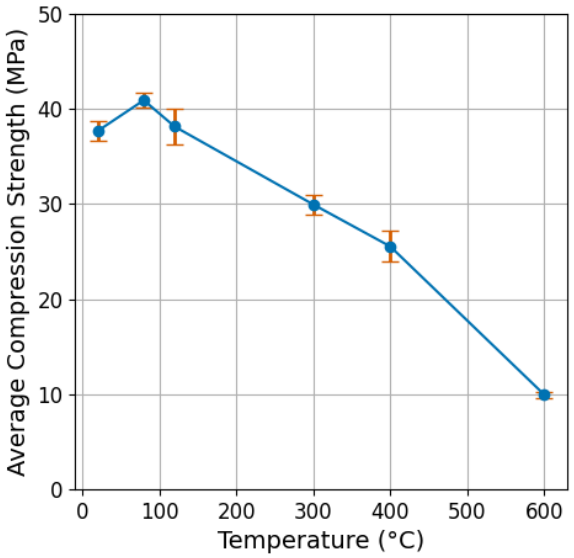

Figure 5: Evolution of compression strength by temperature

4.2.3 Modulus of elasticity

The curves in Figure 6 illustrate a gradual decrease in the modulus of elasticity with increasing temperature. The modulus is calculated in the most linear part of the ascending segment of the stress-strain curve using an automatic routine on compression tests.

From 20°C to 100°C, the elastic modulus decreases slightly. This range corresponds to the evaporation of free water and minimal changes in the microstructure. The loss of stiffness is primarily associated with microcracking due to the combined effect of dehydration and differential thermal expansion between cement paste (which starts shrinking above 100°C) and sand grains (which expand). Between 100°C and

300°C, a more pronounced decrease is observed, with the modulus dropping from 20 GPa to about 12.5 GPa. This decline can be attributed to the dehydration of cementitious phases, notably the C-S-H phase. The microstructure becomes more porous, as reflected in the pore size distribution, resulting in reduced stiffness.

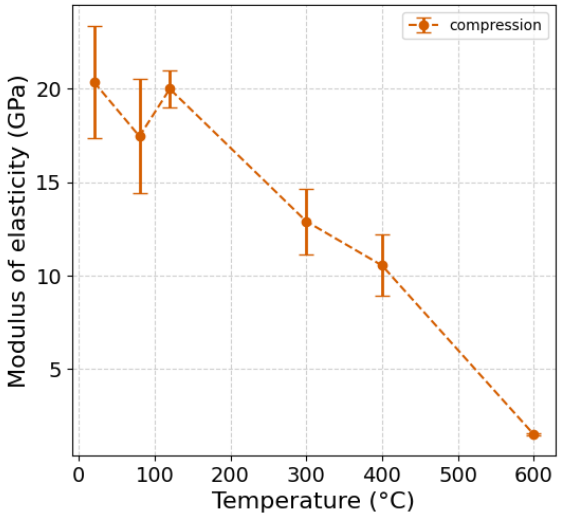

Figure 6: Evolution of modulus of elasticity

From 300°C to 400°C, the reduction in modulus decelerates, reaching approximately 10 GPa. This range corresponds to the decomposition of crystalline phases such as portlandite ($Ca(OH)_2$), transitioning to calcium oxide (CaO). These transformations lead to a significant increase in macropores and cracks. Between 400°C and 600°C, the elastic modulus drops drastically to about 2 GPa. This reflects major structural degradation, associated with the loss of cohesion between the mortar components (accelerated by the quartz transformation at 573°C). This stage is characterized by macroscopic cracking and a complete loss of the material's initial mechanical properties.

The critical temperature range between 300°C and 600°C marks the transition from a partially degraded state to a severely compromised state, where stiffness loss is irreversible. The focus of this study is on the evolution of the modulus with temperature, without performing cyclic loading tests.

4.3 Tests for heat and mass transport properties

4.3.1 Mercury intrusion porosimetry

The pore size distribution curves provide insight into the evolution of the porous microstructure of mortar subjected to temperatures ranging from 80°C to 600°C. The x-axis represents the pore radius (in nm) on a logarithmic scale, while the y-axis indicates the differential pore volume ($\frac{dV}{d\log R}$), figure 7. At 80°C and 120°C, the curves exhibit a primary peak around 100 nm [10]. This peak is sharp and well-defined at 80°C but slightly less pronounced at 120°C. The pores are primarily within the mesopore (2–50 nm) and macropore (>50 nm) ranges, with minimal significant variation observed between these two temperatures.

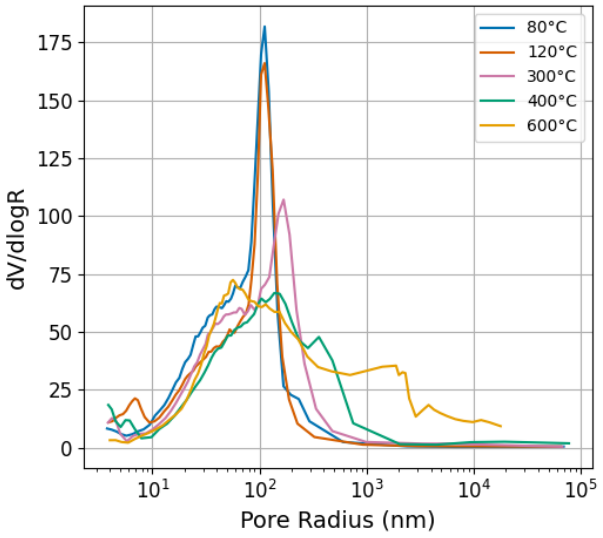

Figure 7: Pore size distribution of mortar by temperature

At 300°C, the primary peak around 100 nm persists but shows reduced intensity compared to 80°C and 120°C. Additionally, an increase in the differential pore volume for smaller pores (around 10 nm) suggests the onset of microstructural changes, likely due to the dehydration of hydrated cement phases, such as calcium silicate hydrate (C-S-H) [4]. At 400°C,

the pore size distribution undergoes significant broadening. The primary peak at 100 nm diminishes further in intensity. Furthermore, there is a notable increase in the volume of larger pores around 1000 nm, indicating the formation of new macropores. These changes correspond to marked thermal degradation, including the decomposition of crystalline phases such as portlandite.

At 600°C, the pore size distribution is drastically altered. The peak at 100 nm is significantly attenuated, reflecting a reduction in dominant mesopores. Additionally, there is a substantial increase in the macropore range (1000–10,000 nm), corresponding to the opening of cracks and loss of material cohesion. These modifications signify advanced structural degradation of the mortar.

4.3.2 Water and mercury porosity

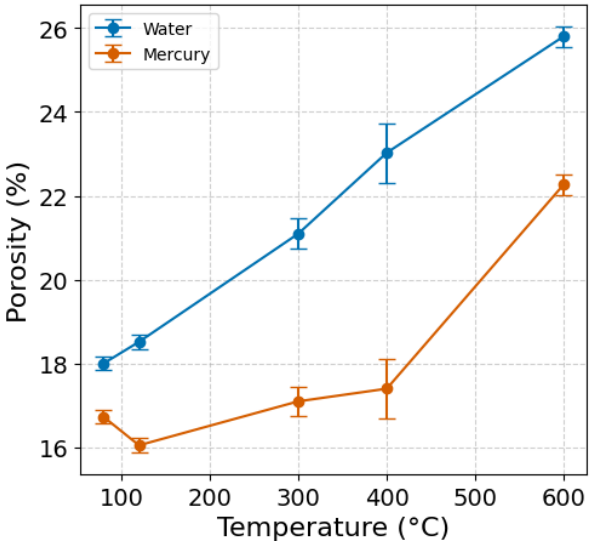

Figure 8: Water and mercury porosity by temperature

With a global observation for the water porosity, the curve show a continual augmentation of the porosity with the temperature with a maximal value around 26% at 600°C. For the mercury porosity, the curve shows a different behavior. The porosity stays quasi constant until 300°C, follows by an notable increase after 400°C, to reach 22% at 600°C 8.

The porosity measured with the water method consistently surpasses the one accessible to mercury. This divergence can be explained by the fact that the water goes into the macro and the micro-pores. In contrast, mercury, because of its high surface tension and the need for high impregnation pressure, can only access larger pores. This difference in wettability and penetration capability means that the water method provides a more comprehensive measurement of total porosity. Additionally, the difference in sample size (approximately 2 grams for mercury intrusion porosimetry versus 130 grams for water porosity measurements for dried samples) may contribute to variations in the measured porosity values (scale factor).

At low temperature (100-300°C), the porosity values don't change a lot, indicating that few new accessible macro-pores appear in this range. At 600 °C, a marked increase in mercury porosity suggests micro-crack formation or opening of pre-existing pore, reflecting a balance between the creation of new micro-pores and the thermal degradation of the material's microstructure.

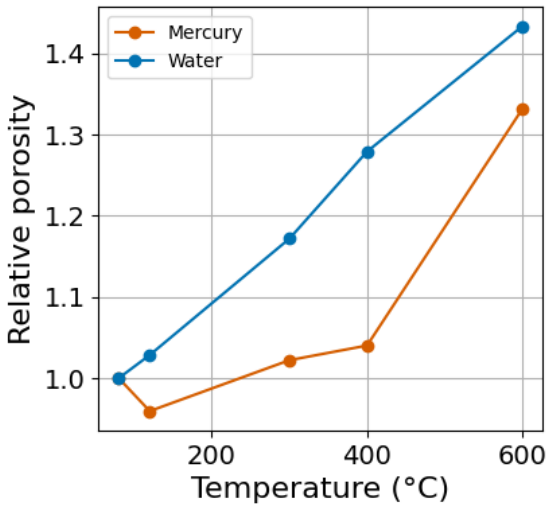

Figure 9: Relative porosity by temperature

Figure 9 illustrates the relative porosity, de-

fined as the ratio of porosity at elevated temperatures to that of the reference state. Between the reference condition and 600°C, the porosity accessible to water demonstrates a 43% increase, while that accessible to mercury exhibits a 33% increase. These values align with porosity trends identified in concrete samples [11].

4.4 Thermal properties

In our experiments, the mortar was in a dry state, which tends to reduce thermal conductivity. The mortar primarily contained quartz aggregates, known for their high thermal conductivity. Based on Jansson's work [12], the tests were conducted on cooled samples.

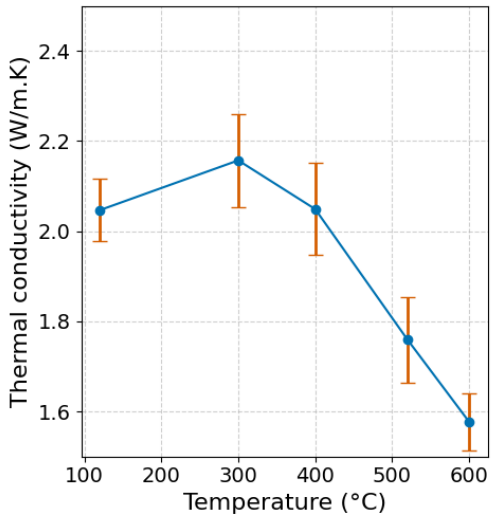

Figure 10: Thermal conductivity per temperature

As shown in Figure 10, thermal conductivity remains relatively stable up to 400°C but decreases significantly beyond this temperature. This decline is attributed to changes in the microstructure. Specifically, the increase in porosity likely introduces air pockets, which act as thermal insulators within the specimens.

The device used in this study (TPS, Transient Plane Source) allows for the evaluation of thermal diffusivity and thermal conductivity. While specific heat capacity (C_p) can be estimated by combining these measurements with assumptions about material density, this approach is less precise. To address this limitation, a complementary campaign using Differential Scanning Calorimetry (DSC) is currently underway. These DSC measurements will provide more accurate specific heat capacity values and further enhance the reliability of our thermal property database.

5 Conclusion

This study thoroughly examines the thermal and mechanical behavior of mortar when exposed to elevated temperatures, focusing on its microstructural changes, mechanical properties, and transport characteristics.

The combined TGA/DSC results reveal phase transformations, such as the dehydration of portlandite and C-S-H gel, and the decarbonation of calcium carbonate, all leading to progressive degradation. These thermal processes directly affect the material's structural integrity, as shown by significant decreases in bending and compressive strengths.

Mechanical tests indicate a notable reduction in stiffness and strength, particularly above 300°C, where thermal damage causes microcracking and the formation of macropores. By 600°C, the mortar retains only a small part of its initial mechanical properties, highlighting its vulnerability to high temperatures. The drop in elastic modulus aligns with observed microstructural changes, confirming the critical temperature range for irreversible mechanical degradation.

Analyzing pore size distribution and porosity demonstrates how thermal exposure alters the mortar's porous network. Mercury intrusion porosimetry finds an increase in macroporosity above 400°C, while water porosity assessments reveal changes at both micro and macro levels. These outcomes emphasize the thermal degradation of cementitious phases and crack propagation, negatively impacting the material's load-bearing capacity and transport properties.

Measurements of thermal conductivity support the effect of microstructural changes on mortar behavior, with increased porosity at higher temperatures introducing air voids that

act as thermal insulators, resulting in a decrease in conductivity above 400°C.

Although these findings provide valuable insight into the high-temperature behavior of cementitious materials, it is important to consider their representativity compared to concrete. Unlike mortar, concrete contains larger aggregates, which significantly influence its thermal and mechanical response. The presence of coarse aggregates can change crack propagation, affect thermal conductivity, and modify the extent of thermal expansion mismatches. Therefore, while the trends observed in this study reflect general cementitious material degradation mechanisms, their direct transposition to concrete must account for aggregate effects and potential differences in scale.

Together, these findings demonstrate the interplay between the thermal, mechanical, and microstructural transformations in mortar under high-temperature conditions. The study emphasizes how phase transformations and the development of porosity influence the material's degradation, offering a robust foundation for future modeling initiatives and better understanding of the fire behavior of cementitious materials.

REFERENCES

[1] Giuseppe Sciumè, 2013, Modèle thermo-hydro-chemo-mécanique du béton au jeune âge et son adaptation pour l'analyse numérique de la croissance des tumeurs cancéreuses, PHD Thesis, UNiversité de Padoué.

[2] Afnor, NF EN 196-1 2016, *Methods of testing cement - Part 1: Determination of strength*; P 15-471-1

[3] Rilem Technical Committees 129-MHT, Test methods for mechanical properties of concrete at high temperatures, Part 1: Introduction, Part 2: Stress–strain relation, Part 3: Compressive strength for service and accident conditions, Materials and Structures 28 (181) (1995) 410–414.

[4] Alonso, C., C. Andrade, et Khoury G.A, 2003. Porosity & Microcracking. Course on effect of heat on concrete.

[5] AFREM, 1997. Compte rendu des journées techniques AFPC-AFREM Durabilité des bétons. Laboratoire Matériaux de Durabilité des Constructions, Institut national des sciences appliquées, Université Paul Sabatier, Toulouse, Décembre 1997.

[6] Gustafsson, S.E. et Long, T., 1995. "Transient Plane Source (TPS) for Measuring Thermal Properties of Building Materials." Fire and Material 19: 43-49.

[7] Hanaa Fares, Sébastien Remond, Albert Noumowe, Annelise Cousture, 2010, High temperature behaviour of self-consolidating concrete Microstructure and physicochemical properties, *L2MGC, Université de Cergy-Pontoise, F-95000 Cergy-Pontoise, France*

[8] Bažant, Z.P., and Cedolin, L. 1996. *Concrete at high temperatures*, Longman Addison-Wesley, London.

[9] M. S. Ghiorso, I. S. E. Carmichael, and L.K. Moret, 1979, Inverted high-temperature quartz: Unit cell parameters and properties of the $\alpha - \beta$ inversion, Department of Geology and Geophysics, University of California, Berkeley, California 94720, USA

[10] Tsimbrovska, M., Kalifa, P., Quenard, D., Daian, J.F.: High performance concretes at elevated temperature: Permeability and microstructure. In: 14th International Conference on Structural Mechanics in Reactor Technology (SMiRT 14) pp. 475–481 (1997)

[11] Jean-Christophe Mindeguia, 2009, Contribution expérimentale à la compréhension des risques d'instabilité thermique des bétons, PHD Thesis, Université de Pau et des Pays de l'Adour.

[12] Jansson R.: Measurement of Concrete Thermal Properties at High Temperature. In: Proceedings from the fib Task Group 4.3 workshop Fire Design of Concrete Structures: What now? What next?, Milan, Italy, 2–3 December 2004

[13] Semsi Yazıcı, Gözde Inan Sezer, Hakan Sengül, 2012, The effect of high temperature on the compressive strength of mortars, Construction and Buildings Materials.

[14] Ana Isabel Marques, João Morais , Paulo Morais, Maria do Rosário Veiga, Carlos Santos, Paulo Candeias, João Gomes Ferreira, 2019, Modulus of elasticity of mortars: Static and dynamic analyses, Construction and Buildings Materials.

[15] B. Weber et al., Heat and mass transfer in heated concrete: evaluation and validation of five numerical models, 2024